ADVANCED OPTICAL MATERIALS
www.advopticalmat.de

ZrO_2 Holographic Metasurfaces for Efficient Optical Trapping in The Visible Range

*Mohammad Biabanifard, Tomasz Plaskocinski, Jianling Xiao, and Andrea Di Falco**

Holographic Metasurfaces (HMs) in the visible range enable advanced imaging applications in compact, planarized systems. The ability to control and structure light with high accuracy and a high degree of freedom is particularly relevant in lab-on-chip biophotonic applications. Pushing the operation wavelength into the blue region and below is an open challenge. Here, it is demonstrated that Zirconium dioxide (ZrO_2) metasurfaces (MSs) are particularly well-suited to satisfy these requirements. Specifically, MSs are designed for optical trapping applications with a high numerical aperture (NA = 1.2) at a wavelength as low as 488 nm, with trap stiffness >200 pN (μmW)$^{-1}$.

1. Introduction

MSs are engineered interfaces, made of arrangements of sub-wavelength meta-atoms, capable of modulating the optical response of the incident light.[1] In HMSs, the meta-atoms act as pixels of a computer-generated hologram. HMSs in the visible range have found applications in virtual and augmented reality, encryption, and security, digital art[2–4] and for imaging and sensing applications.[5–7] In the context of biophotonics applications, MSs can be easily integrated with microfluidic chips[8,9] and used to determine the optical landscape to analyze the specimens of interest, either using a guided configuration or in reflection/transmission at normal incidence,[5,10] with high diffraction efficiency and high spatial frequencies.[11,12] In biophotonics experiments, working in the near-infrared (NIR) is preferred to minimize phototoxicity and reduce the absorption of light in water-based media. Most imaging experiments are instead completed in the visible range, especially to benefit from fluorescence-based assays and increase the imaging resolution, and shorter wavelengths are typically employed to excite fluorophores and dyes.

M. Biabanifard, T. Plaskocinski, J. Xiao, A. Di Falco
School of Physics and Astronomy
University of St Andrews
North Haugh, St. Andrews, Fife KY16 9SS, UK
E-mail: adf10@st-andrews.ac.uk

The ORCID identification number(s) for the author(s) of this article can be found under https://doi.org/10.1002/adom.202400248

DOI: 10.1002/adom.202400248

Visible-light HMSs can be realized with different platforms. HMSs with plasmonic meta-atoms have excellent performance in reflection,[13,14] but they are affected by intrinsic losses, which make their implementation harder in the visible spectrum, and they can complicate the biophotonics experiments due to localized absorption and heat. Silicon-based HMSs have good performance down to the 532 nm region, both in the amorphous phase (a-si)[15] and crystalline phase (c-si), where metalenses with NA up to 1.48 and efficiency >42% were reported.[16–18] TiO_2 HMSs are excellent candidates for applications in the visible range, with reported NA ranging from 0.8 to 1.1 and efficiency from 78% to 50%, respectively,[9,19–21] especially in the crystalline form, which offers high refractive indices. Going to smaller wavelengths, recently, HfO_2 MSs working down to the UV with NA = 0.6 and an efficiency of 60% is reported.[22]

Here we argue that ZrO_2 is a valid and appealing alternative to other platforms for HMSs in the visible range, specifically for biophotonics and optical trapping (OT) applications. It offers a weakly-dispersive and ultra-low loss optical response covering the whole UV and visible range spectrum. Due to its excellent properties, it can be suitable for a variety of purposes across many industries, including biomedical implants,[23] protective coating layers,[24] and optical materials.[25] It is most famously used for hard ceramics,[26] while it is widely used to produce dental implants due to its hardness, chemical inertness, and, most importantly, its biocompatibility.[27] Having excellent resistance to corrosion and different chemicals, very high fracture toughness, high hardness and density, good frictional behavior, low thermal conductivity, and solid electrical insulation make this material interesting to use in light-matter interactions.[28] Also, ZrO_2 takes advantage of fast and very low-temperature deposition. Recently, MSs made with ZrO_2 nanoparticles with the nanoimprinting technique in visible[29] and deep UV spectra have been reported.[30] These ZrO_2 nanoparticles, due to impurity compared with ZrO_2, have a slightly lower refractive index and higher loss in deep UV spectra than bulk ZrO_2.

Here we demonstrate the capability of ZrO_2 to create highly resolved optical landscapes in microfluidics environments by designing HMSs for optical trapping experiments, in the green and blue region of the visible spectrum. The use of HMSs for OT applications is one of the most compelling examples of their versatility. OT is a non-invasive technique providing contactless high-precision manipulation of micron-sized particles[31] and smaller. This is typically achieved by creating suitable optical potentials, for example by strongly focusing Gaussian beams to

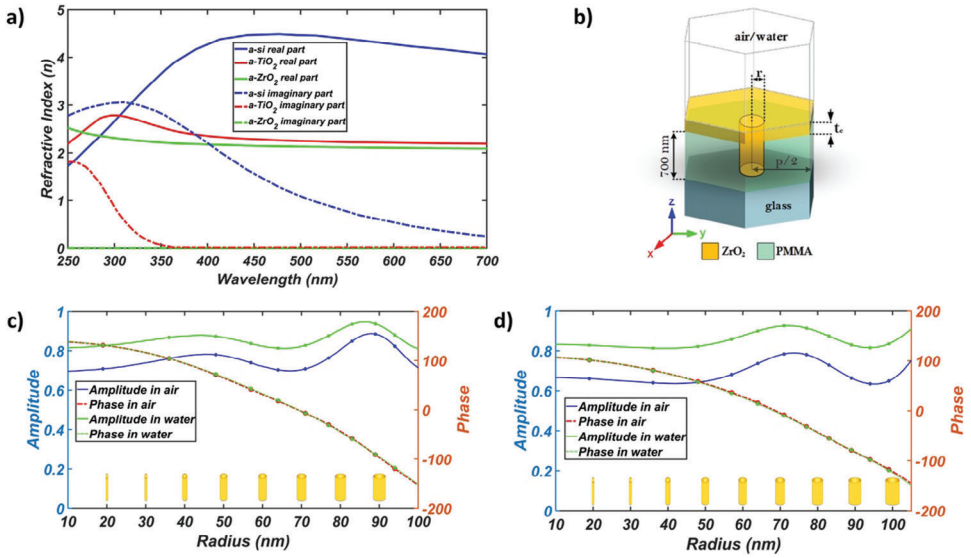

Figure 1. a) Measured refractive index of amorphous ZrO_2 compared with TiO_2, and a-si, b) proposed unit cell perspective, c,d) the transmission and phase profile of meta-atoms in air, and water at 488 nm, and 532 nm, respectively.

spot sizes comparable with the dimensions of the trapped object. The trap stiffness represents the value of the spring constant of the damped oscillator, describing the trapping potential,[32] and depends on the power, wavelength, and optical and geometrical parameters of the trapped object.[33] OT is an efficient method to measure forces in the pN regime, by tracking their effect on the nanometric displacement of the trapped object. This has turned OT into an invaluable tool for investigating biophysical dynamics down to the single molecule level.[34] OT has also been used to directly trap living cells,[35] manipulate nanostructures inside living organisms,[36] in situ assembly of microscopic structures,[37] and manipulate extended objects.[38]

Most of these experiments use bulky, high NA objectives, required to create a balance between the optical scattering and gradient forces applied to the trapped object. Therefore, it is meaningful that MSs technology is starting to be employed for optical trapping applications. In the NIR, it has been demonstrated that metalenses with NA up to 0.88 based on silicon platforms produce a trap stiffness of up to 0.02 pN μm^{-1},[39] or up to 0.013 pN μm^{-1} when using plasmonic-based platforms with NA of 0.7.[40] These Figures of merit have recently been updated to values comparable to that of objectives with NA = 1.2, using a reflective-type MS at 830 nm.[41]

Optical trapping in visible wavelengths, when compared with near-infrared, can provide higher trapping forces (which scale favorably with the inverse of the wavelength used), and better spatial resolution, which is required for the manipulation and control of small objects. However, trapping at shorter wavelengths presents additional challenges because the periodicity of the structure can be comparable with the wavelength of the incident light, thus achieving a high NA is harder. Recently, in the visible range, adaptive Fresnel metalenses using a polymer with NA = 0.88 is patterned on the tip of the optical fiber at the working wavelength of 660 nm, with a trap stiffness of 100 pN $(\mu mW)^{-1}$.[42]

Here, we report on broadband transmissive ZrO_2 HMSs with NA as high as 1.2 in the visible range for on-chip optical trapping and imaging applications, at 488 nm (blue HMSs) and 532 nm (green HMSs), with trapping stiffness of 212 and 130 pN $(\mu mW)^{-1}$ respectively.

2. Experimental Section

2.1. Unit Cell and Hologram Design

Ideally, the MSs should modulate both the amplitude and phase of the scattered light, to create holographic images.[43] However, phase-only holograms, where each meta-atom behaves like the pixel of a digital phase waveplate, produce holograms with sufficiently high efficiencies, using relatively simple architecture. The required phase distribution could be generated with a variety of algorithms, starting from a desired target image. This phase then needs to be mapped to a distribution of suitably chosen meta-atoms. The quality of the holographic image depends on the algorithm used to generate the phase profile and on the diffraction efficiency of the meta-atoms.[44] Here meta-atoms are used that act as truncated waveguides, with dephasing dictated by the different effective refractive indices of the propagating modes.[45,46] The refractive index of the deposited ZrO_2 was measured with an ellipsometer (J.A. Woollam) as shown in **Figure 1a**. The data show that ZrO_2 has a high refractive index that extends from the visible range well into the deep UV region, with negligible absorption. Figure 1b shows a sketch of the unit cells of the HMSs, which are arranged in a hexagonal lattice with a periodicity p of 200 and 210 nm, for the blue and green HMSs respectively. It consists of a thick microscope glass slide as a substrate, a 50 nm thin layer of Indium Tin Oxide (ITO) as a conductive layer, 700 nm tall Zirconium dioxide pillars in a polymethyl methacrylate (PMMA), matrix, and a 180 nm flat layer t_c of ZrO_2 on top.

The design of the meta-atoms was done in COMSOL, where the dispersion data of microscope glass (bk7), ITO, and ZrO_2, were all measured with the ellipsometer. The dispersion data of the PMMA was used from COMSOL Library. In the design, a linearly polarized (E-field on x-axis) plane wave illuminating the structure with normal incidence was considered. To minimize the simulation time, symmetrical boundary conditions along the xz and yz planes were applied, and open space boundaries along the z-axis. Figure 1c,d, illustrates the transmission and phase modulation of the ZrO_2 pillars with different radii at the wavelength of 488 and 532 nm, respectively. The transmission of the meta-atoms was consistently above 80% in water. The phase covers a range of 295° for the blue HMS and 250° for the green HMS, limited by the aspect ratio of the pillars. In the simulations, the case of the dry meta-atoms (in air) were also considered, which was relevant for the HMSs designed to extract the efficiency of the platform experimentally. While the refractive index of the surrounding medium had an impact on the transmission, the phase modulation was the same in both scenarios. This is attributed to the fact that the modes supported by the ZrO_2 meta-atoms were unaffected by the change of the surrounding medium, due to the presence of the planar ZrO_2 layer situated on top of the structure. It is essential to emphasize that the unit-cell approach presented here can be optimized at the desired wavelength within the visible spectrum. To demonstrate the versatility of the platform for applications that go beyond the creation of a tightly focused spot for optical trapping applications, a numerical method was used to design our holographic MSs, rather than using standard metalens designs, with an analytical phase profile.

To design the holograms, a Gerchberg–Saxton (GS) algorithm was used, using a Rayleigh-Sommerfeld propagator between the MS and holographic image plane,[14,47] where the phase of the meta-atoms was discretized in 16 levels, associated with specific pillar radii, as shown in Figure 1c,d, and Tables S1 and S2 (Supporting Information).

2.2. High NA Metasurface Design

The NA of a focusing MS was determined by the Nyquist sampling theorem, so that $NA \leq \lambda/(2P)$, where P and λ are the periodicity of the meta-atoms and the wavelength of the light respectively. Hence, the maximum achievable numerical aperture at 532 nm with 210 nm periodicity is 1.26 as inserted in Figure S1a (Supporting Information). The maximum trapping distance (F) in which $NA = n_m \sin(\varphi)$ is guaranteed, is given by $\mathbf{F} = L\frac{n_m}{2\mathrm{NA}}\sqrt{1-(\frac{\mathrm{NA}}{n_m})^2}$,[48] where φ is the half angle of the focused beam, n_m is the medium refractive index, and L is the side length of the MS.

Figure S1a (Supporting Information) depicts how the ratio ζ = F/L can be selected while ensuring that the periodicity P satisfies the designed numerical aperture. The same considerations apply to the blue HMS case.

2.3. Fabrication

The HMSs were fabricated on a microscope slide, which was cleaned in an ultrasonic bath in acetone and isopropanol, 5 min each. A layer of 50 nm ITO was deposited as a thin conductive layer using a sputterer (Angstrom Engineering) to minimize the electron backscattering effect. A 700 nm-thick layer of PMMA A7 950K (Micro Resist Technology) at 1650 rpm for 60 s was then spin-coated and baked for 5 min at 180 °C. The meta-atoms were defined using a 30 KV Raith eLine Plus Electron Beam Lithography (EBL) Raith Nanofabrication system, followed by 65 s development using a 1:1 ratio of isopropanol and distilled water. This ratio was optimized to ensure all the unit cells with different sizes were fully developed. To verify that this was the case, a sacrificial sample, a layer of gold, and lifted-off were deposited on the PMMA, as shown in Figure S2 (Supporting Information). The sample was then baked for 30 min at 95 °C, and the ZrO_2 layer was deposited via Atomic Layer Deposition (ALD) at a rate of 1.79 Angstroms per cycle.

2.4. Holographic Imaging Setup

Figure S3 (Supporting Information) shows the setup used to collect the images of the HMSs and measure their efficiency in air. A broadband laser (SuperK NKT photonics) was linearly polarized, expanded to a beam with a diameter of 1.5 cm with a telescope made by two lenses with focal length 50 and 400 mm and then focused on the MS with a lens with focal distance 1000 mm. The setup produced a spot size of ≈250 µm diameter at the MS, which had an area of 200 × 200 µm^2. The holographic image was projected at an angle of 30° respect to the normal to the HMS and projected on a screen.

2.5. Optical Trapping Setup

Figure 2 shows a sketch of the trapping setup. The green laser (Laser Quantum, 532 nm) was linearly polarized and expanded to a beam with a diameter of 1.3 cm with a telescope made by two lenses with focal lengths of 100 and 1000 mm. A lens of focal length 1000 mm was used to focus the beam and deliver it via a periscope and a dichroic mirror on top of the MS. This setup produced a spot size of roughly 250 µm in diameter at the 140 × 140 µm^2 MS. The blue laser (Ibeam Toptica, 488 nm) was expanded with a telescope made by two lenses with focal lengths of 35 and 400 mm to a size of 1.3 mm and focused with the same 1000 mm lens. The laser used could be selected with flip mirrors. The sample was imaged with a Nikon microscope (Eclipse Ti-U) with a motorized PRIOR 2D stage. Also, this setup provided a calibration in z-axis where one can trace the movement in z-axis with regards to the image plane. A suitable filter was mounted on the microscope turret to cut the trapping laser while letting the white light reach the CCD camera (Baumer VCXU-13 M), used to record the trapping experiments.

2.6. Trapping Method

To facilitate the trapping experiment, the green light was routed to the back of the microscope and used to trap the SiO_2 beads with a 60X water immersion Microscope (Nikon, PlanAPOVC60xA) objective with NA = 1.2 (see Figure 2). The trapped particle was

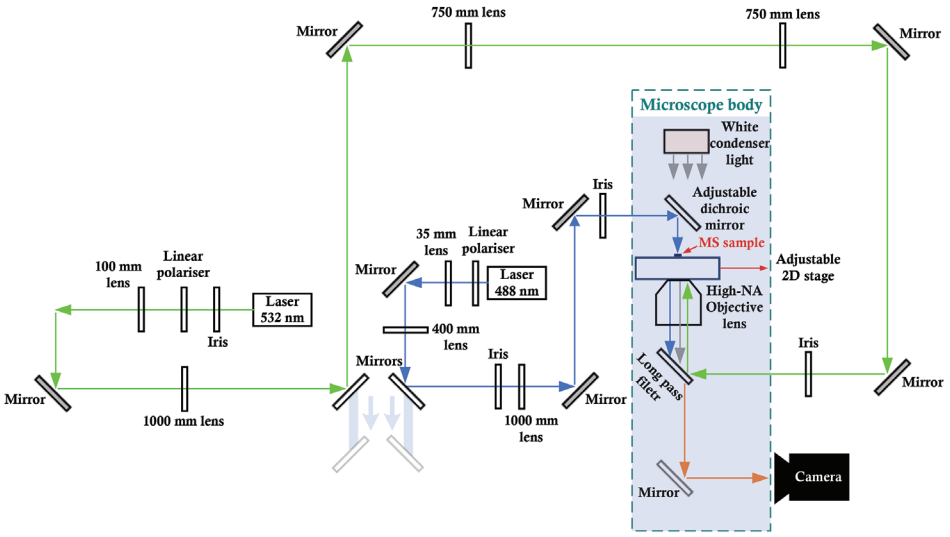

Figure 2. The experimental optical setup used for trapping.

brought in the proximity of the focus of the HMSs before switching the green light off. The calibration of the CCD camera was completed with this objective, which gave a pixel size of 80 nm.

The position trajectories of the particles were extracted from 10-s-long videos acquired at 1000 frames per second (fps) for different laser powers, using a well-established approach, based on the shift properties of the Fourier transform.[49] Typical trajectories for the trapped particles and associated power density spectra are shown in Figure S4 (Supporting Information).

The error bars along the x-axis in Figure 2 are due to the laser power oscillations. The experiments were repeated five times for every single noted power point, giving the error bars in the y-axis for the trap stiffness.

3. Results

Figure 3a depicts a scanning electron microscopy (SEM) image of a fabricated green HMS. It shows encapsulated ZrO_2 meta-atoms, capped with a flat ZrO_2 layer that enables a medium-independent optical response. The figure shows that the walls of the cylinders are not perfectly vertical, which only slightly affects the dephasing of the larger meta-atoms, as shown in Figure S5 (Supporting Information). Given the minor nature of this correction, we decided to neglect this effect. The inset shows a sketch of the section of the HMSs highlighting the Electron beam (E-beam) lithography step used to define the holes in the e-beam resist and the ALD step to create the ZrO_2 nanopillars. To assess the quality of these HMSs, we fabricated two sets of holograms, to measure their efficiency and the image forming capability. For the measurement of the efficiency, we designed HMSs projecting a collimated beam at 30 degrees with respect to the normal to the MS. As customary, the diffraction efficiency was obtained by normalizing the power of the first diffracted orders over the power of the non-diffracted zeroth order, shown in Figure 3b. The error bars indicate how the efficiency is affected by the quality of fabrication, including how well the meta-atoms are exposed and developed. The obtained efficiency of the HMSs is 67% (blue HMS) and 59% (green HMS). The radiation pattern/directivity of the meta-atoms is shown in Figure S6 (Supporting Information). Figure 3c–e depicts the target image and design for holography purposes at 532 nm. A deer-shaped hologram was designed at 30° with respect to the MS normal axis. The simulated holographic image and the corresponding phase profile of the designed hologram are shown in Figure 3d,e, respectively. Figure 3f shows the operation of a structure designed for 532 nm, across the visible range.

For the optical trapping experiments, the HMSs were fabricated on a microscope slide that acts as the ceiling of a microfluidic chip, facing the liquid environment. The HMSs were excited with laser light from the top, to produce focused spots in the microfluidic environment, at distances of 30 and 32 μm at 488 and 532 nm, respectively. The spots and the trapped particles were imaged and analyzed from below, using a CCD camera (see Figure 2). This means that the trapping of the particle is completely independent of its observation. The HMSs were $140 \times 140\ \mu m^2$, thus with nominal NA = 1.22 and NA = 1.21, respectively. The periodicity of each HMS is below the Nyquist limit for this NA.[9] Figure S1a (Supporting Information) shows the geometrical relationship between HMS' area, focal distance, and NA. Figure S1b,d (Supporting Information) shows the phase profile of the HMSs for the two cases.

Figure 4a,b shows the experimental beam profiles at the focal planes for the two HMSs, demonstrating that both lenses have $NA = 0.51\lambda/FWHM \approx 1.2$, where FWHM is extracted from the experimental data. Figure S1c,e (Supporting Information) shows the comparison between the numerical and experimental beam profiles.

To characterize the trap stiffness of the optical trap created by the HMSs we analyzed videos of a trapped SiO_2 particle with a diameter of 2 μm, for different laser powers. The trap stiffness ($K_\perp$), averaged along the x and y directions, is shown in Figure 4c with values of 212 and 130 pN $(\mu W)^{-1}$ at 488 and 532 nm, respectively. The power values used in Figure 4c and in the data analysis are obtained considering the power of the Gaussian beam incident on the MSs, scaled by the geometrical overlap with the HMSs and the efficiency previously measured for both HMSs.

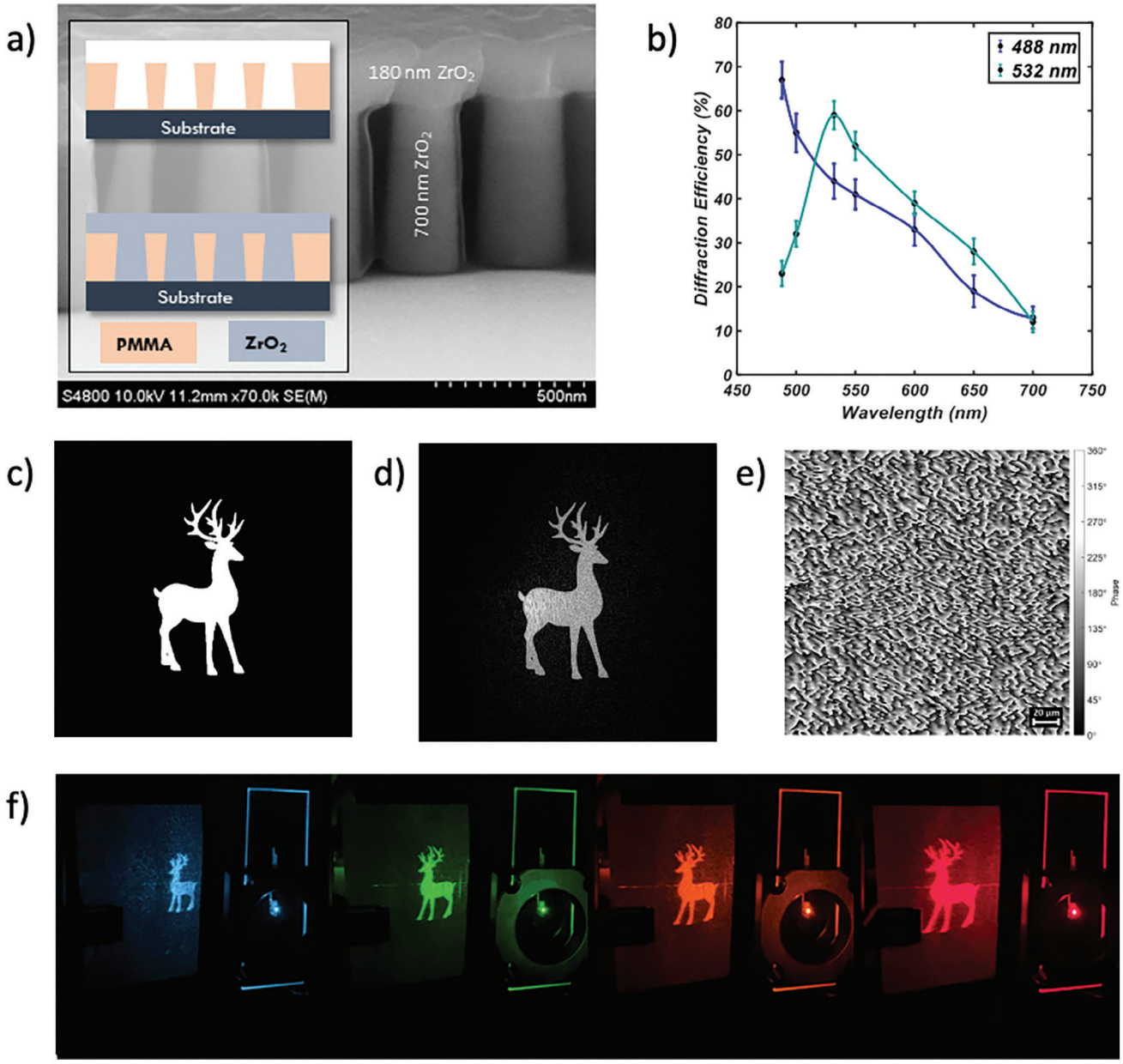

Figure 3. a) SEM image of the fabricated device, inserted are the fabrication work flow consist of EBL and ALD steps, b) the obtained experimental efficiency at visible wavelengths regime, c–f) Visible range broadband response of the MS designed for operation at 532 nm (c) Target image, (d) Designed hologram at 30° respect to the normal axis of MS, (e) the phase profile (f) Experimental holographic image at 488, 532, 590, and 632 nm.

The absolute value for the trap stiffness should be considered in the context of this approximation.

It is important to mention during the experiment with these MSs, by changing the stage position up to more than half an MS side length off-axis, the particle was still trapped, indicating the light is coupled to the structure for this type of transmissive MSs.

4. Discussion

To the best of our knowledge, the results of Figure 4c are the first demonstration of on-chip optical trapping in the blue region. The dependence of the trap stiffness from the wavelength and the trapped object would require a full electromagnetic numerical calculation and its thorough description goes beyond the remit of this work.[50]

Our results show that HMSs provide a high-quality trapping spot, with measured NA limited by the microscope objective used for the collection of the images. It should be noted that we do not expect to be able to exceed meaningfully this value, because the meta-atoms of the HMSs do not cover the full phase space. Additionally, the directionality of their scattering profiles reduces the efficiency of the HMSs for high angles (see Figure S6, Supporting Information), which directly limits the maximum achievable NA.[9] The reduced phase coverage also

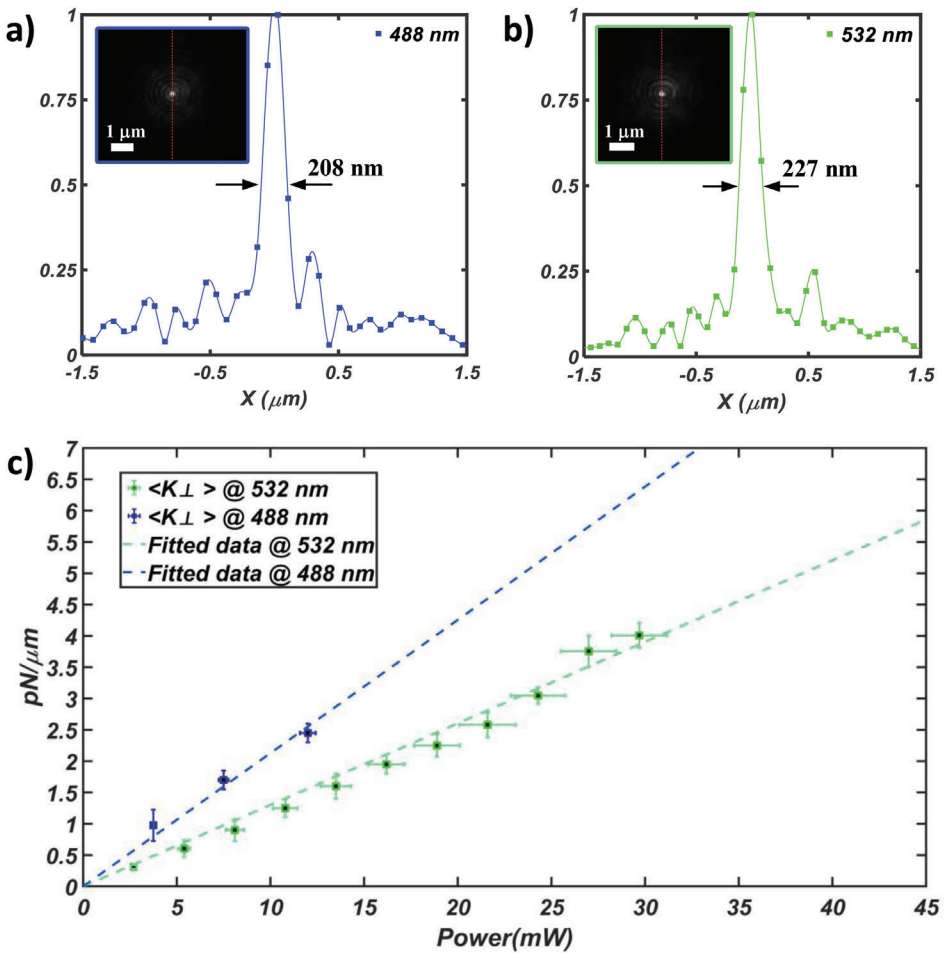

Figure 4. Optical trapping measurements at 488 and 532 nm. a) The experimental beam shape profile at 488 nm with its inserted image at the focal point, b) the experimental beam shape profile at 532 nm with its image at the focal point, and c) the trap stiffness measurements for optical trapping at 488 and 532 nm.

has an impact on the overall diffraction efficiency of the HMSs and on the trap stiffness. This is because the undiffracted light propagates into the chamber, increasing the scattering force acting on the particle. The diffraction efficiency of the HMSs can be improved with further optimization of the meta-atoms design, for example with a more favorable aspect ratio. This puts more stringent requirements in terms of fabrication, which could be satisfied using state-of-the-art nanolithographic approaches.[51]

Here we designed the meta-atoms to be polarization-independent (results not shown), to create a high-quality focused Gaussian beam. If required, HMSs can be designed with polarization-dependent meta-atoms, which could facilitate the creation of optical trapping beams with angular momentum, for optical trapping and manipulation applications with higher degrees of freedom.[52,53]

An advantageous feature of the proposed design is that our structures provide a flat biocompatible layer at the interface with the microfluidic environment, that encapsulates the meta-atoms. Therefore, the response of the meta-atoms is not affected by the medium in which the MS is employed, making it suitable for a wide range of potential biophotonics applications.[48] Additionally, ZrO_2 requires temperature deposition as low as 80 °C, thus making it amenable to integration with polymeric and biophotonic chips.

Finally, ZrO_2 has unique advantages over competing material platforms on the UV range performance,[30] which can be exploited for biological applications in DNA analysis and medical applications.[54,55] These features, along with exceptional material hardness and device robustness, make our HMSs the ideal candidates for on-chip biophotonic integrated applications.

5. Conclusion

We demonstrated ZrO_2 holographic MSs operating in the visible range for holographic imaging and optical trapping purposes. We experimentally reported high numerical aperture ZrO_2 MSs (NA = 1.2) at 488 nm with efficiency >67% and trapping stiffness greater than 200 pN $(\mu mW)^{-1}$. We believe these MSs will be particularly useful in a variety of real-life applications, including holography, optical trapping, and biomedical applications.

Supporting Information

Supporting Information is available from the Wiley Online Library or from the author.

Acknowledgements

The authors thank Dr Graham Bruce for useful discussions on optical trapping experiments. The project was supported by the European Research Council (ERC) under the European Union Horizon 2020 Research and Innovation Program (grant agreement no. 819346).

Conflict of Interest

The authors declare no conflict of interest.

Data Availability Statement

The data that support the findings of this study are openly available in the Data Set of the University of St. Andrews Research Portal at https://doi.org/10.17630/e5371e49-ecc5-42f7-9b74-5dcc96011199.

Keywords

holographic metasurfaces, Optical Trapping, Zirconium dioxide, ZrO_2 nano-antenna

Received: January 27, 2024
Published online:

[1] Y. Nanfang, P. Genevet, M. A. Kats, F. Aieta, J.-P. Tetienne, F. Capasso, Z. Gaburro, *Science* **2011**, *334*, 333.
[2] Y. Libin, J. Xiao, T. Plaskocinski, M. Biabanifard, S. Persheyev, M. Askari, A. Di Falco, *Opt. Express* **2022**, *30*, 19145.
[3] W. Feng, J. Zhang, Q. Wu, A. Martins, Q. Sun, Z. Liu, Y. Long, E. R. Martins, J. Li, H. Liang, *Nano Lett.* **2022**, *22*, 3969.
[4] G.-Y. Lee, J.-Y. Hong, S. H. Hwang, S. Moon, H. Kang, S. Jeon, H. Kim, J.-H. Jeong, B. Lee, *Nat. Commun.* **2018**, *9*, 4562.
[5] S. Zhang, C. L. Wong, S. Zeng, R. Bi, K. Tai, K. Dholakia, M. Olivo, *Nanophotonics* **2020**, *10*, 259.
[6] Y. Jahani, E. R. Arvelo, F. Yesilkoy, K. Koshelev, C. Cianciaruso, M. D. Palma, Y. Kivshar, H. Altug, *Nat. Commun.* **2021**, *12*, 3246.
[7] Y. Sun, C. Wang, S. Zheng, X. Tao, X. Liu, Y. Li, F. Wu, Z. Zheng, *Sci. Rep.* **2022**, *12*, 20476.
[8] M. L. Tseng, H.-H. Hsiao, C. H. Chu, M. K. Chen, G. Sun, A.-Q. Liu, D. P. Tsai, *Adv. Opt. Mater.* **2018**, *6*, 1800554.
[9] W. T. Chen, A. Y. Zhu, M. Khorasaninejad, Z. Shi, V. Sanjeev, F. Capasso, *Nano Lett.* **2017**, *17*, 3188.
[10] Y. Qin, Y. Li, D. Deng, Y. Liu, M. Sun, *Appl. Opt.* **2019**, *58*, 4438.
[11] E. Ostroff, K. Parekh, A. Prominski, B. Tian, *Adv. Mater. Technol.* **2022**, *7*, 2100216.
[12] Z. Terzopoulou, A. Zamboulis, I. Koumentakou, G. Michailidou, M. J. Noordam, D. N. Bikiaris, *Biomacromolecules* **2022**, *23*, 1841.
[13] G. Zheng, H. Mühlenbernd, M. Kenney, G. Li, T. Zentgraf, S. Zhang, *Nat. Nanotechnol.* **2015**, *10*, 308.
[14] J. Burch, A. Di Falco, *ACS Photonics* **2018**, *5*, 1762.
[15] S. Gao, C.-S. Park, S.-S. Lee, D.-Y. Choi, *Adv. Opt. Mater.* **2019**, *7*, 1801337.
[16] H. Liang, Q. Lin, X. Xie, Q. Sun, Y. Wang, L. Zhou, L. Liu, X. Yu, J. Zhou, T. F. Krauss, J. Li, *Nano Lett.* **2018**, *18*, 4460.
[17] Z. Zhou, J. Li, R. Su, B. Yao, H. Fang, K. Li, L. Zhou, J. Liu, D. Stellinga, C. P. Reardon, T. F. Krauss, X. Wang, *ACS Photonics* **2017**, *4*, 544.
[18] J. Zhang, H. Liang, Y. Long, Y. Zhou, Q. Sun, Q. Wu, X. Fu, E. R. Martins, T. F. Krauss, J. Li, X. Wang, *Laser Photonics Rev.* **2022**, *16*, 2200268.
[19] R. C. Devlin, M. Khorasaninejad, W. Ting Chen, J. Oh, F. Capasso, *Proc. Natl. Acad. Sci. USA* **2016**, *113*, 10473.
[20] W. T. Chen, A. Y. Zhu, V. Sanjeev, M. Khorasaninejad, Z. Shi, E. Lee, F. Capasso, *Nat. Nanotechnol.* **2018**, *13*, 220.
[21] M. Khorasaninejad, W. T. Chen, R. C. Devlin, J. Oh, A. Y. Zhu, F. Capasso, *Science* **2016**, *352*, 1190.
[22] C. Zhang, S. Divitt, Q. Fan, W. Zhu, A. Agrawal, Y. Lu, T. Xu, H. J. Lezec, *Light: Sci. Appl.* **2020**, *9*, 55.
[23] S. Gupta, S. Noumbissi, M. F. Kunrath, *Med. Devices Sens.* **2020**, *3*, e10076.
[24] Z. Sagdoldina, B. Rakhadilov, M. Skakov, O. Stepanova, *Mater. Test.* **2019**, *61*, 304.
[25] Y. Pan, *J. Electron. Mater.* **2019**, *48*, 5154.
[26] A. El-Ghany, O. Saleh, A. H. Sherief, *Future Dental J.* **2016**, *2*, 55.
[27] M. Hisbergues, S. Vendeville, P. Vendeville, *J. Biomed. Mater. Res., Part B* **2009**, *88*, 519.
[28] W. M. Ahmed, T. Troczynski, A. P. McCullagh, C. C. L. Wyatt, R. M. Carvalho, *J. Esthet. Restor. Dent.* **2019**, *31*, 423.
[29] M. Miyata, A. Kohno, T. Komatsu, T. Hashimoto, *Opt. Mater. Express* **2022**, *12*, 4169.
[30] J. Kim, W. Kim, D. K. Oh, H. Kang, H. Kim, T. Badloe, S. Kim, C. Park, H. Choi, H. Lee, J. Rho, *Light: Sci. Appl.* **2023**, *12*, 68.
[31] A. Ashkin, *Phys. Rev. Lett.* **1970**, *25*, 1321.
[32] N. Malagnino, G. Pesce, A. Sasso, E. Arimondo, *Opt. Commun.* **2002**, *214*, 15.
[33] A. Ashkin, *Proc. Natl. Acad. Sci. USA* **1997**, *94*, 4853.
[34] T. T. Perkins, *Annu. Rev. Biophys.* **2014**, *43*, 279.
[35] A. Ashkin, J. M. Dziedzic, T. Yamane, *Nature* **1987**, *330*, 769.
[36] P. L. Johansen, F. Fenaroli, L. Evensen, G. Griffiths, G. Koster, *Nat. Commun.* **2016**, *7*, 10974.
[37] J. E. Melzer, E. McLeod, *Microsyst. Nanoeng.* **2021**, *7*, 45.
[38] M. Askari, B. C. Kirkpatrick, T. Čižmár, A. D. Falco, *Opt. Express* **2021**, *29*, 14260.
[39] G. Tkachenko, D. Stellinga, A. Ruskuc, M. Chen, K. Dholakia, T. F. Krauss, *Opt. Lett.* **2018**, *43*, 3224.
[40] H. Markovich, I. I. Shishkin, N. Hendler, P. Ginzburg, *Nano Lett.* **2018**, *18*, 5024.
[41] J. Xiao, T. Plaskocinski, M. Biabanifard, S. Persheyev, A. Di Falco, *ACS Photonics* **2023**, *10*, 1341.
[42] M. Plidschun, H. Ren, J. Kim, R. Förster, S. A. Maier, M. A. Schmidt, *Light: Sci. Appl.* **2021**, *10*, 57.
[43] G.-Y. Lee, G. Yoon, S.-Y. Lee, H. Yun, J. Cho, K. Lee, H. Kim, J. Rho, B. Lee, *Nanoscale* **2018**, *10*, 4237.
[44] L. Huang, S. Zhang, T. Zentgraf, *Nanophotonics* **2018**, *7*, 1169.
[45] P. Lalanne, *J. Opt. Soc. Am. A* **1999**, *16*, 2517.
[46] S. M. Kamali, A. Arbabi, E. Arbabi, Y. Horie, A. Faraon, *Nat. Commun.* **2016**, *7*, 11618.
[47] R. W. Gerchberg, W. O. Saxton, *Optik* **1972**, *37*, 237.
[48] R. Geromel, C. Weinberger, K. Brormann, M. Tiemann, T. Zentgraf, *Opt. Mater. Express* **2022**, *12*, 13.
[49] I. T. Leite, S. Turtaev, X. Jiang, M. Šiler, A. Cuschieri, P. S. J. Russell, T. Čižmár, *Nat. Photonics* **2018**, *12*, 33.
[50] P. H. Jones, O. M. Maragò, G. Volpe, *Optical Tweezers: Principles and Applications*, Cambridge University Press, Cambridge **2015**.
[51] K. J. Morton, G. Nieberg, S. Bai, S. Y. Chou, *Nanotechnology* **2008**, *19*, 345301.
[52] T. Plaskocinski, Y. Arita, G. D. Bruce, S. Persheyev, K. Dholakia, A. Di Falco, H. Ohadi, *Appl. Phys. Lett.* **2023**, *123*, 081106.
[53] D. Cojoc, V. Garbin, E. Ferrari, L. Businaro, F. Romanato, E. Di Fabrizio, *Microelectron. Eng.* **2005**, *78*, 125.
[54] J. Tamariz, K. Voynarovska, M. Prinz, T. Caragine, *J. Forensic Sci.* **2006**, *51*, 790.
[55] S. Gorog, *Ultraviolet-Visible. Spectrophotometry in Pharmaceutical Analysis*, CRC press, Boca Raton, Florida **1995**.